Consistent definitions for, and relationships among, cross sections for elastic scattering of hydrogen ions, atoms, and molecules

Predrag S. Krstić and David R. Schultz
Physics Division, Oak Ridge National Laboratory, Oak Ridge, Tennessee 37831-6372
(Received 8 March 1999)

Owing to the crucial role played by elastic scattering in various gas/plasma environments and to its fundamental nature, we consider in the present work low-energy collisions among isotopic variants of $H^+ + H$, $H + H$, and $H^+ + H_2$. In particular, we present consistent definitions of the elastic-scattering cross section and its common transport relevant moments regarding the quantum indistinguishability or classical distinguishability of particles, correcting some inappropriate definitions found in the literature. Further, we utilize a large collection of fully quantal calculated results for these systems to display the scaling relationships that exist among them. [S1050-2947(99)01309-8]

PACS number(s): 34.50.−s, 34.10.+x

I. INTRODUCTION

The transport of particles and, in particular, the exchange of momentum, in cool hydrogen plasma/gas can be dominantly determined by elastic scattering among hydrogen ions, atoms, and molecules. For example, recent emphasis on the engineering design of fusion reactors has focused attention on these issues regarding the so-called divertor region in which high-density, low-temperature hydrogen plasma is produced to bring about the neutralization and heat exhaust from the burning plasma in the core region [1–7]. Furthermore, elastic scattering has been shown to be an important process in numerous astrophysical environments, for example, in planetary ionospheres [8], the heliospheric shock at the interface of our solar system and the local interstellar medium [9,10], comet bow shocks (see, e.g., [11]), and nonradiative shocks in supernovae ejecta (see, e.g., [12]). Interest generated by the recent experimental observations of Bose-Einstein condensates has also spurred the need for accurate description of very-low-temperature elastic scattering (e.g., for H+H scattering, see [13,14]).

Noting these needs for a comprehensive understanding of elastic and related transport cross sections, and due to the considerable inconsistency in the literature regarding the definitions of these quantities in some cases, and their applications, we present here an exposition of consistent definitions and an analysis of the cross-section scaling relationships among various hydrogen species collision systems.

In particular, there has been considerable inconsistency in the definition of the elastic (el) cross section as well as its higher moments, the momentum transfer (mt) and viscosity (vi) cross sections, with respect to the quantum indistinguishability of colliding particles (QIP) in symmetric systems such as $H^+ + H$ or H+H [15–21,13]. This indistinguishability is manifested by an overlap of the wave functions at low collision energies and thus by significant interference between the elastic and charge transfer channels in the case of ion-atom scattering, or by the direct elastic and recoil channels for the atom-atom case. With increasing collision energy, the overlap decreases and pronounced peaks for forward and backward scattering are displayed by the differential cross sections. These peaks correspond in this limit to elastic scattering (forward) and either charge transfer (backward) for the ion-atom case or target recoil (backward) for the atom-atom case, and thus enabling classical distinguishability of the particles (CDP), i.e., labeling of the projectile and the target. An experiment in the low collision energy limit would not have the means of distinguishing the two overlapping channels by scattering angles or the projectile energy; the only means left for labeling the projectile and target are spins of the colliding nuclei.

Since, in practice, most experiments, as well as plasma modeling, assume unpolarized beams of projectiles and unpolarized targets, the relevant theory of elastic scattering should take into account the spin statistics of the nuclei [18,15,21]. This results in an elastic cross section which, for high collision energies, tends to the ''total'' cross section for scattering of projectiles, rather than to the elastic one, thus representing an experiment in which direct and recoil channels are not separated even for energies where CDP is in effect. Particularly sensitive to this definition is the momentum transfer cross section, derived by integration of the elastic differential cross section weighted by $1-\cos\theta$, where θ is the scattering angle. Since the weighting factor emphasizes the backward scattering angles, the momentum transfer cross section could be considerably larger if recoil scattering is present in the elastic cross section in the case when the target particles are included.

Thus the definition of the elastic cross section as well as of its higher moments for the symmetric (nuclei) systems do not have the classical limit, defined by CDP, even when the latter can be reached in an experiment. Alternately, the inability to distinguish projectiles ions from ions coming from the target by charge transfer (ct) leads one to define the ''spin-exchange'' (se) cross section, assuming the scattering of a polarized beam of projectiles on an unpolarized target [15,21]. If the scattered particle is detected with changed nuclear spin, and spin coupling is not present, this particle has certainly come from the target. The spin exchange cross section does have the correct classical limit, which would smoothly become equivalent to the charge transfer cross section in the CDP limit. One may analogously define the spin

exchange cross section for identical atom-atom scattering [18,13,22].

Two significantly different sets of elastic and transport cross sections could be produced for the symmetric collision systems even at higher energies, depending on the assumption of QIP or CDP. Although each of the sets is internally consistent, they could potentially introduce a confusion in plasma modeling applications, resulting in double counting. For example, if QIP is used in modeling of the ion (neutral) transport, the resulting momentum transfer cross section contains both contributions from elastic and symmetric charge transfer (recoil) processes, and thus the charge transfer contribution must be removed from the transport code. Since most of the transport applications rely on the CDP, it is important to define the meaning of ''low'' (where QIP is assumed) and ''high'' energies (where CDP is adequate). Without removing the QIP in calculations for symmetric systems, we define in Sec. II quantities that have correct CDP limits for elastic, momentum transfer, and viscosity cross sections and estimate the errors of using the CDP assumption over the center-of-the-mass (CM) collision energy range considered. Also significant is the result that quantities defined in this way enable a unique scaling and meaning of all elastic and transport cross sections within each type of collision system, irrespective of isotopic constitution.

Four types of systems, ion-atom ($A^+ + B$), atom-atom ($A + B$), ion-molecule ($A^+ + BC$), and atom-molecule ($A + BC$), have been studied, where A, B, and C are any of the hydrogen atom isotopes (H, D, or T). The hydrogen molecules are assumed to be initially in their ground vibrational state. These constitute 51 distinct collision systems. We base our conclusions on recent [23,24] fully quantal calculations of more than 2800 differential and more than 200 integral cross sections spanning the CM collision energy range of 0.1–100 eV. Besides utilizing the best available potential energy surfaces and carefully checking numerical convergences to achieve high accuracy in the calculations, the good quality of the data was also verified by extensive comparison with the theoretical and experimantal data available in the literature. These comparisons have been presented elsewhere [23,24]. Scaling relations among the integral elastic and transport cross sections are described in Sec. III. Atomic units (a.u.) are used throughout the text unless stated otherwise.

II. CALCULATION OF THE ELASTIC AND TRANSPORT CROSS SECTIONS

Calculation of these differential and integral cross sections has been described in detail recently [23,24] and only the essential features of the numerical methods are summarized briefly here. For example, common to the calculational techniques for all systems considered is the solution of the relevant Schrödinger radial equation or system of equations (in cases that involve molecular targets). These have been solved using the method described by Johnson [25] based on the use of the logarithmic derivative. The step size used in the numerical mesh was between 0.001 and 0.0001 while the convergence of a solution for the elastic amplitude a_ℓ in the number of partial waves, ℓ, was established for each energy by requiring that $1-\mathrm{Re}\{a_\ell\} \leqslant 10^{-5}$, $\mathrm{Im}^2\{a_\ell\} \leqslant 10^{-5}$ for at least ten successive partial waves. The number of partial waves needed for convergence of the elastic amplitudes was usually significantly larger than the amount needed for the corresponding convergence of inelastic amplitudes, reflecting the importance of the region of large internuclear distance R in elastic scattering. The converged amplitudes were matched to the standard plane-wave boundary conditions in order to define the K matrix and subsequently the unitarized S matrix [25]. This was then used to define the elastic phase shifts δ_ℓ, where $S_\ell = \exp(i2\delta_\ell)$. The differential cross sections were calculated for 768 CM scattering angles in interval $(0,\pi)$, starting from angles as small as 6×10^{-6} rad to facility Gauss-Legendre quadrature.

We used QIP where appropriate (i.e., for the symmetric collision pairs) in the definition of the elastic differential cross sections $d\sigma/d\Omega$, while for ion-atom and atom-atom systems which involved different isotopic constituents, the projectile and target nuclei were, of course, considered as distinguishable at all energies, thus satisfying CDP. The integral elastic cross section, σ_{el}, and its higher moments [26], momentum transfer σ_{mt} and viscosity σ_{vi}, were found by numerical and (where possible) analytic integration over scattering angles,

$$\sigma_{\mathrm{el}} = 2\pi \int_0^\pi d\theta \sin\theta \frac{d\sigma}{d\Omega}, \tag{1}$$

$$\sigma_{\mathrm{mt}} = 2\pi \int_0^\pi d\theta \sin\theta (1-\cos\theta) \frac{d\sigma}{d\Omega}, \tag{2}$$

$$\sigma_{\mathrm{vi}} = 2\pi \int_0^\pi d\theta \sin^3\theta \frac{d\sigma}{d\Omega}. \tag{3}$$

Comparisons of the two methods of the integration yielded agreement better than four significant digits. The calculated differential and integral cross sections, as well as those for charge transfer and spin exchange, can be reviewed in both graphical and tabular forms [42]. In the following we briefly explain the details of the calculations of the cross sections, specific for each of the four system types.

A. Hydrogen ion-atom collision systems: $A^+ + B$

Adiabatic potential energy surfaces for H_2^+ can be found with arbitrary accuracy, using separation of variables in prolate elliptic coordinates [27] for this two-center, one-electron system. We calculated the ground gerade and ungerade potential curves ($1s\sigma$ and $2p\sigma$) and their first derivatives for all $R \leqslant 1$ with steps of 0.0001 and for $R \leqslant 50$ with steps of 0.001 to obtain smooth linear fits for values of R needed by the radial Schrödinger equation solver. For even larger R, the analytic asymptotic expansion of the potentials [28] up to eleventh order in $1/R$ was used.

If the masses of the projectile and target are different, as is the case with isotopically different nuclei, the asymptotic energies of the $1s\sigma$ and $2p\sigma$ split for the difference in binding energies of A and B, induced by a small difference in the electron reduced mass for the two atoms. This small difference in masses can be transformed into a difference in charges of the two nuclei [29], thus destroying exact gerade-ungerade symmetry. Still, the splitting in the levels is so

TABLE I. Parameters in Eq. (11) for spin-averaged integral elastic cross sections in symmetric ion-atom systems.

				$H^+ + H, T^+ + T$				$D^+ + D$			
Type	g	η_1	η_2	ω_1^+	ω_2^+	ω_1^-	ω_2^-	ω_1^+	ω_2^+	ω_1^-	ω_2^-
Total	$2\ell+1$	δ_ℓ^g	δ_ℓ^u	$\frac{1}{4}$	$\frac{3}{4}$	$\frac{3}{4}$	$\frac{1}{4}$	$\frac{2}{3}$	$\frac{1}{3}$	$\frac{1}{3}$	$\frac{2}{3}$
Momentum transfer	$\ell+1$	$\delta_\ell^g-\delta_{\ell+1}^u$	$\delta_\ell^u-\delta_{\ell+1}^u$	$\frac{1}{4}$	$\frac{3}{4}$	$\frac{3}{4}$	$\frac{1}{4}$	$\frac{2}{3}$	$\frac{1}{3}$	$\frac{1}{3}$	$\frac{2}{3}$
Viscosity	$\frac{(\ell+1)(\ell+2)}{2\ell+3}$	$\delta_{\ell+2}^g-\delta_\ell^g$	$\delta_{\ell+2}^u-\delta_\ell^u$	$\frac{1}{4}$	$\frac{3}{4}$	$\frac{3}{4}$	$\frac{1}{4}$	$\frac{2}{3}$	$\frac{1}{3}$	$\frac{1}{3}$	$\frac{2}{3}$

small (0.0037 eV for the HD^+ system) that it results in a negligible effect for collision energies of 0.1 eV and greater, resulting in approximate identity (four digits) of the cross sections for $A^+ + B$ and $B^+ + A$ scattering. Thus we assume that an approximate gerade-ungerade symmetry of the AB^+ wave functions is preserved, while the nuclei are distinguishable. We include the small effect of the mass difference in the adiabatic potentials [30]. These assumptions yield for the integral cross sections [15]

$$\sigma_{\rm el}=\frac{\pi}{k^2}\sum_{\ell=0}^{\infty}(2\ell+1)[\sin^2\delta_\ell^g+\sin^2\delta_\ell^u + 2\sin\delta_\ell^g\sin\delta_\ell^u\cos(\delta_\ell^g-\delta_\ell^u)], \tag{4}$$

$$\sigma_{\rm ct}=\frac{\pi}{k^2}\sum_{\ell=0}^{\infty}(2\ell+1)\sin^2(\delta_\ell^g-\delta_\ell^u), \tag{5}$$

$$\sigma_{\rm mt}=\frac{\pi}{k^2}\sum_{\ell=0}^{\infty}(\ell+1)(\sin^2\Delta_\ell^g+\sin^2\Delta_\ell^u + \sin\delta_{\ell+1}^g\sin\delta_\ell^u\cos\Delta_\ell^{gu}+\sin\delta_{\ell+1}^u\sin\delta_\ell^g\cos\Delta_\ell^{ug}), \tag{6}$$

$$\sigma_{\rm vi}=\frac{\pi}{k^2}\sum_{\ell=0}^{\infty}\frac{(\ell+1)(\ell+2)}{2\ell+3}(\sin^2\Gamma_\ell^g+\sin^2\Gamma_\ell^u + \sin\delta_{\ell+2}^g\sin\delta_\ell^u\cos\Gamma_\ell^{gu}+\sin\delta_{\ell+2}^u\sin\delta_\ell^g\cos\Gamma_\ell^{ug}), \tag{7}$$

where k is the CM momentum, $\Delta_\ell^a=\delta_{\ell+1}^a-\delta_\ell^a$, $\Delta_\ell^{ab}=\delta_{\ell+1}^a-\delta_\ell^b$, $\Gamma_\ell^a=\delta_{\ell+2}^a-\delta_\ell^b$, $\Gamma_\ell^{ab}=\delta_{\ell+2}^a-\delta_\ell^b$, for each partial wave ℓ, and a and b stand for either u or g. The charge transfer cross section, $\sigma_{\rm ct}$, is well defined under CDP even at low energies.

As discussed in the Introduction, if the nuclei are identical and the collision energy is low enough, there is no way to distinguish which ion is elastically scattered and which ion results from charge transfer from the target nuclei, unless we label the particles by their spin. But in a typical situation of an unpolarized projectile beam and target, we must account for the appropriate spin statistics, which yields ''elastic'' cross sections that contain contributions from both channels coherently. With the increase of collision energy, these evolve into the ''total'' scattering cross sections for the projectiles.

This may be formalized by first defining the relative CM motion of the nuclei by the vector $\vec{R}=\vec{R}_1-\vec{R}_2$. The interchange of particles results in the change of the sign $\vec{R}\to-\vec{R}$, or, equivalently, the change of scattering angle θ into $\pi-\theta$ while $\vec{R}$ is unchanged. The detector at angle θ counts both particles scattered at θ and $\pi-\theta$. When nuclei have the same charge but are distinguishable by other means, the scattering amplitudes for the direct elastic, $f_d(\theta)$, and charge transfer, $f_{\rm ct}(\theta)$, channels are commonly defined in terms of scattering amplitudes on uncoupled gerade and ungerade ground states [15,20], i.e.,

$$f_d(\theta)=\frac{f_g(\theta)+f_u(\theta)}{2} \tag{8}$$

and

$$f_{\rm ct}(\theta)=\frac{f_g(\theta)-f_u(\theta)}{2}. \tag{9}$$

These amplitudes are used to define the differential cross sections for scattering when the two nuclei are different isotopes of hydrogen. In a fully symmetric case, taking into account spin statistics of an unpolarized beam on an unpolarized target, one obtains [15,20,21]

$$\frac{d\sigma_{\rm tot}}{d\Omega}=s_1|f_d(\theta)-f_{\rm ct}(\pi-\theta)|^2+s_2|f_d(\theta)+f_{\rm ct}(\pi-\theta)|^2, \tag{10}$$

where $s_1=\frac{3}{4}$ and $s_2=\frac{1}{4}$ in the case of protons and tritons (fermions), and $s_1=\frac{1}{3}$ and $s_2=\frac{2}{3}$ in the case of deuterons (bosons). We use subscript ''tot'' for the cross section in Eq. (10), rather than the usual ''el,'' thus stressing the true meaning of the equation in the CDP limit: incoherent combination of ''el'' and charge transfer. On the other hand, assuming a polarized incident beam, one defines the amplitude for spin exchange [20,21] as $f_{\rm se}(\theta)=f_{\rm ct}(\theta)$, Eq. (9). The spin exchange obviously acquires the meaning of the charge transfer amplitude when CDP is applicable, therefore from here forward we will use the subscript ''ct'' for either charge transfer or spin exchange.

For the symmetric (sym) ion-atom systems, performing integration over scattering angles analytically, the formulas obtained for the integral elastic cross section and its higher moments take the same form

$$\sigma_{\rm tot,sym}=\frac{4\pi}{k^2}\sum_{\ell=\pm}g(\ell)(\omega_1^\pm\sin^2\eta_1+\omega_2^\pm\sin^2\eta_2), \tag{11}$$

where the coefficients are summarized in Table I, for conve-

nience, while

$$\sigma_{\mathrm{ct,sym}}=\frac{4\pi}{k^2}\sum_{\ell=0}^{\infty}(2\ell+1)\sin^2(\delta_\ell^g-\delta_\ell^u). \tag{12}$$

The cross sections, defined by Eq. (11) and Table I, do not tend to those of Eqs. (4), (6), and (7) even when the energy is high enough that the amplitudes in Eq. (10) add incoherently (CDP limit). For example, $\sigma_{\mathrm{tot,sym}}^{(\mathrm{el})}$ for H_2^+ is approximately a factor of $\sqrt{2}$ larger than σ_{el} calculated for H_2^+ using Eq. (4), over almost the entire range of energies considered, although both are referred to as ''elastic'' cross sections in the literature. Still, it is possible to construct an elastic cross section even for symmetric systems, which has the correct CDP limit and, as we show in Sec. III, has a reasonable interpretation even at energies as low as 0.1 eV. In the rest of the text we will call this the ''elastic'' cross section for symmetric ion-atom scattering, i.e.,

$$\sigma_{\mathrm{el,sym}}=\sigma_{\mathrm{tot,sym}}^{\mathrm{el}}-\sigma_{\mathrm{ct,sym}}. \tag{13}$$

To define the momentum transfer and viscosity cross sections with the correct CDP limit, it is convenient to define the ''elastic'' differential cross section by subtracting $d\sigma_{\mathrm{ct,sym}}/d\Omega$ from $d\sigma_{\mathrm{tot,sym}}/d\Omega$ and applying the weighted integration in Eqs. (2) and (3) to the resulting $d\sigma_{\mathrm{el}}/d\Omega$ to obtain the form

$$\begin{aligned}\frac{d\sigma_{\mathrm{el}}}{d\Omega}&=s_1|f_d(\theta)-f_{\mathrm{ct}}(\pi-\theta)|^2+s_2|f_d(\theta)+f_{\mathrm{ct}}(\pi-\theta)|^2\\&\quad-|f_{\mathrm{ct}}(\pi-\theta)|^2\\&=|f_d(\theta)|^2-2(s_1-s_2)f_d(\theta)f_{\mathrm{ct}}(\pi-\theta).\end{aligned} \tag{14}$$

The integral elastic cross section of Eq. (13) is compatible with the definition in Eq. (14).

Obviously, the elastic differential cross section so defined for a symmetric system differs from the CDP cross section by the interference term, which vanishes in the CDP limit. Although $d\sigma_{\mathrm{el}}/d\Omega$ can be negative for some angles and energies, at least in principle, it results in integral cross sections with the correct CDP limit, as we illustrate in Sec. III.

B. Hydrogen atom-atom collision systems: $A+B$

The $H(1s)+H(1s)$ collision system evolves along the ground singlet $X^1\Sigma_g^+$ and triplet $b^3\Sigma_u^+$ potentials, which become degenerate when $R\to\infty$. If various H isotopes constitute the system, then the singlet and triplet states split in the asymptotic limit for the same reasons as in the A^++B case. We find that the mass asymmetry affects only the fifth digit and beyond in the integral elastic cross section, which is for all practical purposes insignificant. The required H_2 potentials were obtained from Jamieson [31], who compiled, fitted, and extrapolated the data of Kolos and Wolniewicz [32]. Although these potentials are not as accurate as those for H_2^+, they represent the best data currently available. More detail regarding the calculation of elastic cross sections for the neutral, atom-atom scattering will be given elsewhere [24].

The symmetric systems (like H + H, D + D, and T + T) also require in this case special attention. In the absence of other means, we again use the spin to label the identical nuclei at lower energies, where the overlap of the direct and recoil channels is significant. Two kinds of spin statistics are involved in the problem here, one with respect to the electron spins and another with respect to nuclear spins. Thus, assuming scattering of an unpolarized beam of atoms by an unpolarized target, and applying the proper nuclear spin statistics and symmetrization of the amplitudes, we obtain the ''elastic'' differential cross sections for the electronic singlet (s) and triplet (t) states separately in the form [18,13]

$$\begin{aligned}\frac{d\sigma_{s,t}}{d\Omega}&=\xi_{H_2}[a_{s,t}|f_{s,t}(\theta)+f_{s,t}(\pi-\theta)|^2\\&\quad+b_{s,t}|f_{s,t}(\theta)-f_{s,t}(\pi-\theta)|^2],\end{aligned} \tag{15}$$

where $a_s=1/4$, $b_t=3/4$, $a_t=1/4$, and $b_t=3/4$ for hydrogen and tritium atoms, and $a_s=2/3$, $b_s=1/3$, $a_t=1/3$, and $b_t=2/3$ for deuterium atoms. Taking into account the statistics of the electron singlet and triplet spin states, the ''elastic'' differential cross section finally takes the form

$$\frac{d\sigma_{\mathrm{el}}}{d\Omega}=\frac{1}{4}\frac{d\sigma_s}{d\Omega}+\frac{3}{4}\frac{d\sigma_t}{d\Omega}. \tag{16}$$

This contains contributions from both scattered and recoiled atoms, and due to the full symmetry between the projectile and the target, the differential cross section is symmetrical about the scattering angle $\pi/2$, i.e., forward and backward peaks are identical. Therefore, the integral elastic cross section for a symmetric system is a factor of 2 larger than the one obtained assuming CDP, described by scattering of, for example, isotopically different particles. Thus we adopt the factor $\xi_{H_2}=1/2$, which guarantees the correct CDP limit of the integral elastic cross section, still keeping interference of the forward and backward peaks in the differential cross section. The factor ξ_{H_2} also affects the momentum transfer and viscosity cross sections, but does not bring them to the correct CDP limit. The solution to this problem is discussed in Sec. III.

The integral cross sections can be written in the form [13]

$$\sigma=\xi_{H_2}\frac{4\pi}{k^2}\sum_{\ell=\pm}g(\ell)(\omega_1^{\pm}\sin^2\eta_1+\omega_2^{\pm}\sin^2\eta_2), \tag{17}$$

where the coefficients $g(\ell)$, $\omega_{1,2}^{\pm}$, and $\eta_{1,2}$ are given in Table II. We note that elastic and momentum transfer cross sections here are identical. This follows directly from consistent use of the defining relation, Eq. (2) with Eq. (15), and is a consequence of the specific nature of the sums in partial waves (either even or odd sums) and of the orthogonality properties of Legendre polynomials. This definition of the momentum transfer cross section describes diffusion of both elastically scattered and recoiled H atoms, compatible with the QIP nature of the process. The coefficients for the elastic and viscosity cross sections are identical to those obtained by Jamieson *et al.* [13]. However, their momentum transfer cross section is calculated with the use of the Boltzmann spin

TABLE II. Parameters in Eq. (17) for spin-averaged integral elastic cross sections in symmetric atom-atom systems.

				$H+H,T+T$					$D+D$		
Type	g	η_1	η_2	ω_1^+	ω_2^+	ω_1^-	ω_2^-	ω_1^+	ω_2^+	ω_1^-	ω_2^-
Elastic	$2\ell+1$	δ_ℓ^s	δ_ℓ^t	$\frac{1}{4}$	$\frac{9}{4}$	$\frac{3}{4}$	$\frac{3}{4}$	$\frac{2}{3}$	1	$\frac{1}{3}$	2
Momentum transfer	$2\ell+1$	δ_ℓ^s	δ_ℓ^t	$\frac{1}{4}$	$\frac{9}{4}$	$\frac{3}{4}$	$\frac{3}{4}$	$\frac{2}{3}$	1	$\frac{1}{3}$	2
Viscosity	$\frac{(\ell+1)(\ell+2)}{2\ell+3}$	$\delta_{\ell+2}^s-\delta_\ell^s$	$\delta_{\ell+2}^t-\delta_\ell^t$	$\frac{1}{4}$	$\frac{9}{4}$	$\frac{3}{4}$	$\frac{3}{4}$	$\frac{2}{3}$	1	$\frac{1}{3}$	2

statistics [31] and is therefore incompatible with Eq. (15). This inconsistency has been recently corrected [14].

When the nuclei are of different masses we consider them as CDP, so that the cross sections can be calculated by considering scattering without regard to the nuclear spins. This yields the differential cross section

$$\frac{d\sigma_{\rm el}}{d\Omega}=\frac{1}{4}|f_s(\theta)|^2+\frac{3}{4}|f_t(\theta)|^2, \tag{18}$$

where $f_{s,t}(\theta)$ are the amplitudes for scattering on the singlet and triplet potentials. For the integral cross sections we obtain

$$\sigma_{\rm el}=\frac{4\pi}{k^2}\sum_{\ell=0}^{\infty}(2\ell+1)\left(\frac{1}{4}\sin^2\delta_\ell^s+\frac{3}{4}\sin^2\delta_\ell^t\right), \tag{19}$$

$$\sigma_{\rm mt}=\frac{4\pi}{k^2}\sum_{\ell=0}^{\infty}(\ell+1)\left(\frac{1}{4}\sin^2\Delta_\ell^s+\frac{3}{4}\sin^2\Delta_\ell^t\right), \tag{20}$$

and

$$\sigma_{\rm vi}=\frac{4\pi}{k^2}\sum_{\ell=0}^{\infty}\frac{(\ell+1)(\ell+2)}{2\ell+3}\left(\frac{1}{4}\sin^2\Gamma_\ell^s+\frac{3}{4}\sin^2\Gamma_\ell^t\right), \tag{21}$$

where $\Delta_\ell^a=\delta_{\ell+1}^a-\delta_\ell^a$, $\Gamma_\ell^a=\delta_{\ell+2}^a-\delta_\ell^a$, and a and b stand for either s or t.

C. Hydrogen ion-, atom-molecule collision systems: $A^+,A+BC$

When the collision time is much shorter than the characteristic rotation time of the diatomic molecular target, one may consider the molecular orientation fixed during the collision [infinite order sudden approximation (IOSA) [33–35]]. This condition is approximately fulfilled for the hydrogen molecule in the CM collision energy range presently considered, i.e., for 0.1–100 eV. As a consequence the diatomic vibrational coordinate ρ and reactive coordinate R (between the projectile and the diatomic center of the mass) suffice to describe the collision dynamics [35]. The ensemble average is performed on the cross sections over diatomic orientation γ (angle between $\vec{\rho}$ and $\vec{R}$), treated as a parameter during a collision.

In the atom-molecule cases (H_3), only the ground singlet potential surface was needed in this calculation. The *ab initio* calculation of the ground potential surface of H_3 presents serious difficulties because of the high degree of symmetry in the system. We calculated the ground potential adiabatic surface using a 54-state Gaussian basis in unrestricted Hartree-Fock, full configuration interaction calculations using GAMESS [36], over a range of $R,\rho\leqslant 1$, on a numerical mesh with a step of 0.1, and for angles γ in interval of 0°–180° with steps of 10°. This was then smoothly connected with the excellent analytical surface fit of Boothroyd [37], for $R\leqslant 10$, and continued for large R with the asymptotic, analytic potential of the van der Waals type. The same basis was used for calculation of the H_3^+ potentials, though both ground $H^+ + H_2$ and first excited (the ground of $H+H_2^+$) adiabatic surfaces were needed in this case. This is due to a strong avoided crossing between the two potential surfaces of H_3^+ at $\rho\simeq 2.6$, for all $R>4.5$. Thus if the neutral molecular target H_2 is in a high vibrational state ($\nu\geqslant 4$), the H_3^+ makes an almost diabatic transition to the excited surface upon collision, resulting in charge transfer, $H+H_2^+$.

To account for this effect of ''crossing'' of the H_3^+ surfaces, we transformed the two electronic adiabatic surfaces to diabatic surfaces with correct boundary conditions, following the procedure developed by Baer [34], using the diatom-in-molecule method (DIM) nonadiabatic matrix elements, needed in transformation. The DIM method is sufficiently accurate for larger R's (where the nonadiabatic seam occurs). The calculation of the potential was done on a numerical mesh with a step of 0.1 in range of ρ between 0.1 and 6 and of R between 0 and 15, for the same γ's as in the H_3 case. At even larger R we approximated the potential with dipole and polarization corrections [38,39].

Finally, only the ground diabatic surface, corresponding to the $H^+ + H_2$ at $R\rightarrow\infty$ (elastic channel), was then used in the scattering calculations. The same H_3 and H_3^+ ground surfaces were used in calculations for all isotopic variations of the target (H_2, HD , D_2, HT, DT, and T_2) and the projectile (H^+,D^+, and T^+). The mass effect was included in the calculation of the vibrational wave functions by solving the radial Schrödinger equation on the relevant diatomic potentials. These functions were needed for excited vibrational-vibrational matrix elements on the ground electronic surfaces. The R-dependent matrix elements were fitted by cubic splines for each γ, and in that form these were used in solving the resulting truncated Schrödinger equation, for various partial waves of the projectile. This constitutes a system of coupled second-order differential equations for the partial wave amplitudes, which we solve by the Johnson algorithm of logarithmic derivatives [25]. Excited vibrational states up to $\nu\leqslant 9$ were included in the calculation of the elastic cross section for both atom-molecule and ion-molecule elastic scattering on the ground vibrational ($\nu=0$) state. Even at an energy of 100 eV, the nine vibrational states were sufficient

to achieve convergence of the elastic cross section and its transport moments. The number of partial waves for each collision energy was increased until convergence was achieved for the elastic amplitude in five significant digits. We note that the maximum number $\ell_{\max}$ of the partial waves needed for the elastic amplitudes exceeds by almost a factor of 2 the number needed for convergence of the inelastic (vibrational excitation) amplitudes with the same accuracy. The $\ell_{\max}$ showed a weak dependence upon diatomic orientation γ. Detailed description of the results of the calculation is given elsewhere [23,24].

Given the vibrational amplitudes $a_\nu(\infty,\gamma,\ell)$, the differential cross section for elastic scattering on the ground vibrational state is [35]

$$\frac{d\sigma_{\rm el}(E)}{d\Omega}=\frac{1}{8k^2}\sum_{\ell}\sum_{\ell'}(2\ell+1)(2\ell'+1)\times P_\ell(\cos\theta)P_{\ell'}(\cos\theta)\times\int_0^\pi d\gamma\,\sin\gamma[1-a_0(\infty,\gamma,\ell)]\times[1-a_0^*(\infty,\gamma,\ell')], \tag{22}$$

where $\vec{k}$ is the initial CM momentum and E the corresponding kinetic energy, $E=k^2/2$, δ is the Kronecker symbol, and the limit $R\to\infty$ is assumed. Finally, the integral elastic cross section was obtained by integration over the full scattering solid angle Ω, which yields

$$\sigma_{\rm el}(E)=\frac{\pi}{2k^2}\sum_{\ell}(2\ell+1)\int_0^\pi d\gamma\,\sin(\gamma)|1-a_0(\infty,\gamma,\ell)|^2. \tag{23}$$

The momentum transfer and viscosity cross sections were calculated by numerical integration of Eq. (22), with the appropriate θ-dependent weights [Eqs. (2) and (3)]. Both differential and integral cross sections show good agreement with those available from other authors [35,39–41].

III. SCALING RELATIONS

For the ion-atom and atom-atom systems we performed semiclassical calculations [6] in addition to the fully quantal treatments. The agreement of the two sets of the results, already at the level of phase shifts, showed that the energy range considered is well within the region of semiclassical validity. Thus, a reasonable primitive quantity characterizing the elastic cross sections is the semiclassical phase shift, δ_ℓ. For small-angle scattering on short-range potentials it has been shown that these scale directly with the square of the relative collision velocity [16]. As shown below, the same type of scaling is present for the integral elastic cross sections for all collision systems considered, even when molecular targets are involved. However, we have found no appropriate scaling for the differential cross sections applicable for the whole range of the scattering angles.

A. Hydrogen ion-atom collision systems: $A^+ + B$

We recall that the cross sections for symmetric systems ($A^+ + A, A = \mathrm{H, D, T}$) were calculated taking into account the indistinguishability of the nuclei, which we call here case (α). At high energies the ''elastic'' cross section in this prescription tends to the total scattering cross section $\sigma_{\rm tot,sym}$, while the spin exchange cross sections becomes the common symmetric charge transfer cross section, $\sigma_{\rm ct,sym}$. On the other hand, for the cases where the projectile and target nuclei are distinguishable, case (β), for example when these differ isotopically, both elastic and charge transfer cross sections have their original meaning for all collision energies. In order to remediate this apparent inconsistency in possible applications, we defined in Sec. II also a ''pure'' elastic cross sections for case (α), as the difference of $\sigma_{\rm tot,sym}$ and $\sigma_{\rm ct,sym}$, that is, $\sigma_{\rm el,sym}=\sigma_{\rm tot,sym}-\sigma_{\rm ct,sym}$. This has two features: (i) It smoothly tends to the elastic cross section of the case (β); (ii) the variation of $\sigma_{\rm el,sym}$ from the one in case (β) is an appropriate measure of the distinguishability of like nuclei, in the energy range considered. We present next the scaling relations for all of the definitions.

In case (α) both the total and spin-exchange (which we call ''charge transfer'' to emphasize its ''semiclassical'' limit) cross sections scale as

$$\sigma_{\rm tot,sym}^{A^+ + A}(E)=\sigma_{\rm tot,sym}^{\mathrm{H}^+ + \mathrm{H}}\left(\frac{\mu_0}{\mu_{AA}}E\right), \tag{24}$$

$$\sigma_{\rm ct,sym}^{A^+ + A}(E)=\sigma_{\rm ct,sym}^{\mathrm{H}^+ + \mathrm{H}}\left(\frac{\mu_0}{\mu_{AA}}E\right), \tag{25}$$

where μ_{AA} is the reduced mass of $A^+ + A$ (μ_0 is the reduced mass of $\mathrm{H}^+ + \mathrm{H}$). When isotopically different nuclei are involved, case (β), both charge transfer and elastic cross sections scale as in the symmetric case, Eqs. (24) and (25). Concerning the relation between these two groups of cross sections, the scaled elastic cross sections of the type (β) match approximately the $\mathrm{H}^+ + \mathrm{H}$ one when multiplied by $\sqrt{2}$, i.e.,

$$\sqrt{2}\,\sigma_{\rm el}^{A^+ + B}(E)=\sigma_{\rm tot,sym}^{\mathrm{H}^+ + \mathrm{H}}\left(\frac{\mu_0}{\mu_{AB}}E\right) \tag{26}$$

while for charge transfer we have

$$\sigma_{\rm ct}^{A^+ + B}(E)=\sigma_{\rm ct}^{\mathrm{H}^+ + \mathrm{H}}\left(\frac{\mu_0}{\mu_{AB}}E\right). \tag{27}$$

Assuming $\sigma_{\rm tot,sym}=\sigma_{\rm el,sym}+\sigma_{\rm ct,sym}$, as in Eq. (13), one obtains from Eqs. (24)–(27),

$$\sigma_{\rm ct}^{A^+ + A}(E)=\frac{\sqrt{2}-1}{\sqrt{2}}\sigma_{\rm tot,sym}^{A^+ + A}(E), \tag{28}$$

i.e., $\sigma_{\rm ct}^{A^+ + B}(E)=(\sqrt{2}-1)\sigma_{\rm el}^{A^+ + B}(E)$, for any A and B. Finally, considering all elastic cross sections (including $\sigma_{\rm el,sym}$), the scaling with the reduced mass is obtained, i.e.,

$$\sigma_{\rm el}^{A^+ + B}(E)=\sigma_{\rm el}^{\mathrm{H}^+ + \mathrm{H}}\left(\frac{\mu_0}{\mu_{AB}}E\right) \tag{29}$$

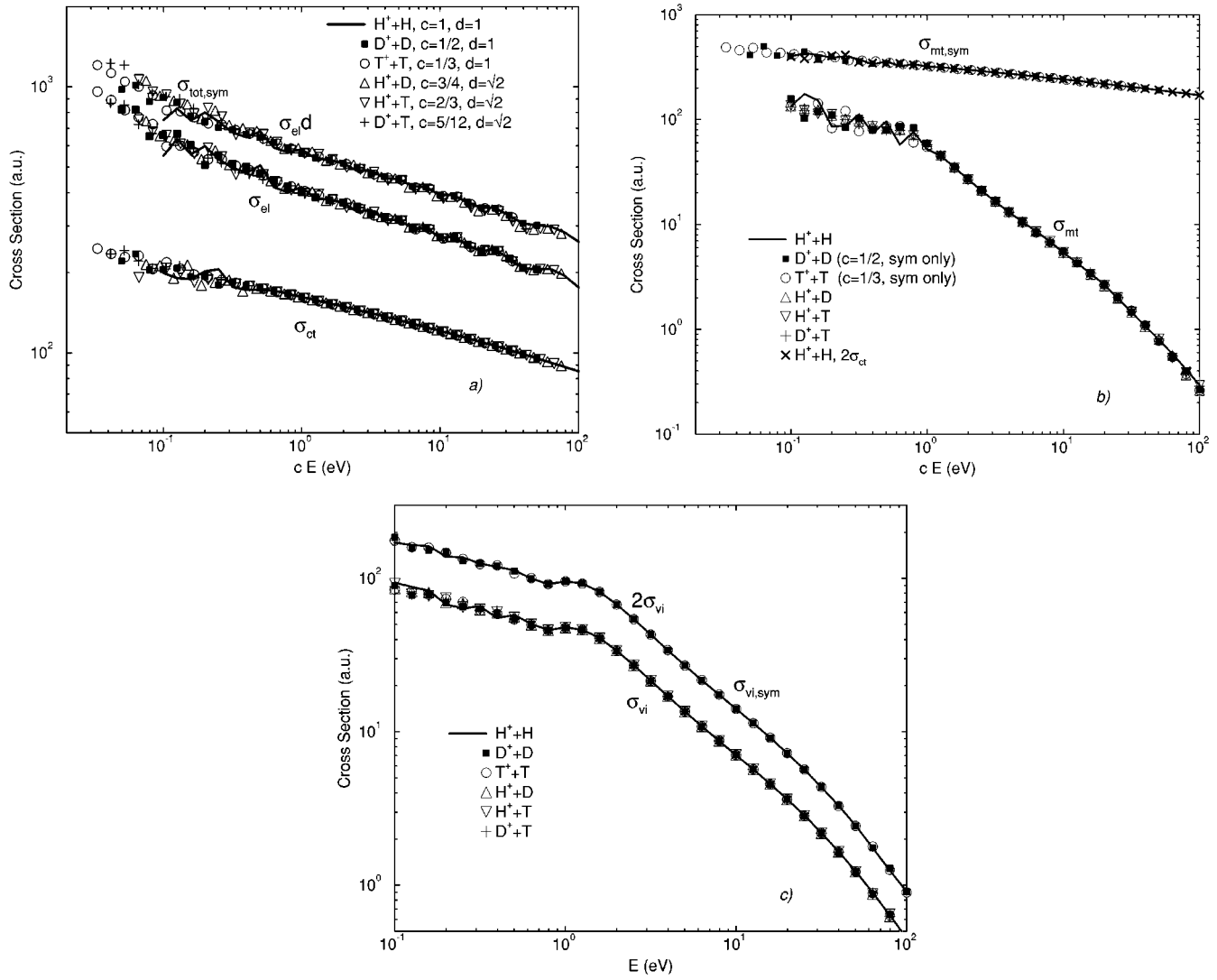

FIG. 1. Scaling of the cross sections for the isotopic variants of hydrogen ion-atom collision systems: (a) elastic, symmetric ($\sigma_{\mathrm{tot,sym}}$, see the text), asymmetric (σ_{el}), and charge transfer (σ_{ct}); (b) momentum transfer, symmetric ($\sigma_{\mathrm{mt,sym}}$), and asymmetric (σ_{mt}); and (c) viscosity, symmetric ($\sigma_{\mathrm{vi,sym}}$), and asymmetric (σ_{vi}). The $H^+ + H$ case is indicated by a solid line. For concreteness, we note that the atomic unit of length squared (i.e., for the cross section) is the Bohr radius squared, $a_o^2 = 8.7954 \times 10^{-17}\ \mathrm{cm}^2 = 1$ a.u.

for all A and B. The above results are demonstrated graphically in Fig. 1(a). The scaled charge transfer cross sections for all of the systems lie within 1% of one another for CM collision energies above 0.5 eV. At lower energies, where interference effects of the elastic and charge transfer channels are significant, the scaling deteriorates. Still, the cross sections oscillate with approximately the same mean value. The elastic cross sections (σ_{el}) reach a 1% scaling accuracy if the collision energy is above 1 eV, with a maximum deviation of 5% at 0.5 eV, and about 25% at 0.1 eV.

As for the elastic cross sections, the momentum transfer cross sections for the symmetric cases, even in the CDP limit, can be defined for two possible types of situations of type (α), in which one does not distinguish between the scattered projectiles and ions produced in the target and of type (β), where only scattered projectiles are counted. Thus, either $d\sigma_{\mathrm{tot,sym}}/d\Omega$ [as in Eq. (10), type (α)] or $d\sigma_{\mathrm{el,sym}}/d\Omega$ [as in Eq. (13), type (β)] is used in defining the momentum transfer cross section, Eq. (2). Momentum transfer cross sections obtained using $d\sigma_{\mathrm{el,sym}}/d\Omega$ for symmetric systems almost coincide with those obtained for asymmetric cases, as shown in Fig. 1(b). In this event no scaling is needed, i.e.,

$$\sigma_{\mathrm{mt}}^{A^+ + B}(E) = \sigma_{\mathrm{mt}}^{\mathrm{H}^+ + \mathrm{H}}(E). \tag{30}$$

For energies above 1 eV the agreement is within 1% and below that energy the deviations are of the order of the interference oscillation amplitudes (15%). On the other hand, momentum transfer cross sections defined by $d\sigma_{\mathrm{tot,sym}}/d\Omega$ scale with the reduced mass, similarly to the elastic and charge transfer cross sections, i.e.,

$$\sigma_{\mathrm{mt,sym}}^{A^+ + A}(E) = \sigma_{\mathrm{mt,sym}}^{\mathrm{H}^+ + \mathrm{H}}\left(\frac{\mu_0}{\mu_{AA}}E\right). \tag{31}$$

The scaled cross sections do not deviate more than 5% in the whole energy range considered.

Finally, in Fig. 1(b) we also show the level of compliance of these results with the known relation

$$\sigma_{\mathrm{mt,sym}}^{A^+ + A}(E) \approx 2\sigma_{\mathrm{ct}}^{A^+ + A}(E) \tag{32}$$

valid for systems with indistinguishable nuclei, for the whole energy range. The agreement is within 0.1% for energies above 1 eV. Although Fig. 1(b) shows only the $H^+ + H$ case, it is obvious that the relation stays valid for the $D^+ + D$ and $T^+ + T$ systems. Taking into account Eqs. (26)–(28), we augment this relation with another useful relation

$$\sigma_{\mathrm{mt,sym}}^{A^+ + A}(E) \approx (2 - \sqrt{2})\sigma_{\mathrm{tot,sym}}^{A^+ + A}(E). \tag{33}$$

The viscosity cross sections calculated for both cases (α) and (β) are independent of the reduced mass, and no scaling is needed [Fig. 1(c)]. It is interesting to note that a simple relation between the (α) and (β) cross sections is valid over the whole energy range, i.e.,

$$\sigma_{\mathrm{vi,sym}}(E) \approx 2\sigma_{\mathrm{vi}}(E), \tag{34}$$

reflecting the factor of 2 between the two definitions of the differential cross sections at a scattering angle of $\pi/2$. Thus

$$\sigma_{\mathrm{vi,sym}}^{A^+ + A}(E) = \sigma_{\mathrm{vi,sym}}^{\mathrm{H}^+ + \mathrm{H}}(E), \tag{35}$$

$$\sigma_{\mathrm{vi}}^{A^+ + B}(E) = \sigma_{\mathrm{vi}}^{\mathrm{H}^+ + \mathrm{H}}(E). \tag{36}$$

Below 0.5 eV, the cross sections deviate from each other by at most 7%. We note that the lower curves in Fig. 1(c) also include the symmetric cases, calculated from Eq. (13).

B. Hydrogen atom-atom collision systems: $A + B$

The cross sections for symmetric systems ($A + A, A = \mathrm{H,D,T}$) were calculated taking into account the indistinguishability of the nuclei [case (α)]. As discussed in Sec. II, the integral elastic cross sections that comply with the correct CDP limit are obtained from case (α) by simple division by 2, to account for the symmetry of the differential cross section in the center of the mass with respect to the direct (forward) and backward (recoil) scattering. This is reflected by the curves in Fig. 2(a), where, upon scaling of the collision energy with mass, all elastic cross sections, either calculated from Eq. (16) or Eq. (19), approximately coincide. Their agreement is better than 1% at energies above 1 eV but does not become worse than 12% at 0.1 eV. The interference oscillations in the cross sections are significantly smaller in comparison to the ion-atom cases due to the absence of the charge transfer channel and due to the short-range nature of the interaction potential. The total spin exchange cross sections, after scaling of collision energy with the reduced mass, group along two separate curves, one for the distinguishable and one for the indistinguishable nuclei cases. These are almost parallel and can be reduced to one curve by division of the QIP cross sections by approximately $d = 1 + \sqrt{3}$, as shown in Fig. 2(a). All these relations are summarized by the following formulas:

$$\sigma_{\mathrm{el}}^{A+B}(E) = \sigma_{\mathrm{el}}^{\mathrm{H+H}}\left(\frac{\mu_0}{\mu_{AA}}E\right), \tag{37}$$

$$\sigma_{\mathrm{se}}^{A+B}(E) = \frac{1}{d\,\sigma_{\mathrm{se,sym}}^{\mathrm{H+H}}}\left(\frac{\mu_0}{\mu_{AA}}E\right), \tag{38}$$

where μ_0 is the reduced mass of H + H, $d = 1 + \sqrt{3}$ for the symmetric systems, and $d = 1$ otherwise.

Scaling of the momentum transfer cross sections needs to be considered separately for the cases (α) and (β), which is a consequence of a pronounced backward peak in the ''elastic'' cross section for symmetric cases. As discussed in Sec. II, the momentum transfer cross section calculated from Eq. (16) is equal to the elastic cross section, Fig. 2(b). This scales, as the elastic one, with the reduced mass, i.e.,

$$\sigma_{\mathrm{mt,sym}}^{A+A}(E) = \sigma_{\mathrm{mt,sym}}^{\mathrm{H+H}}\left(\frac{\mu_0}{\mu_{AA}}E\right). \tag{39}$$

On the other hand, for the case of isotopically different nuclei one can use Eq. (20) to evaluate the momentum transfer cross sections. The resulting cross sections are isotopically invariant. Thus, the assumption of the CDP for both symmetric and asymmetric cases yields

$$\sigma_{\mathrm{mt}}^{A+B}(E) = \sigma_{\mathrm{mt}}^{C+D}(E), \tag{40}$$

where A, B, C, and D are any combination of H, D, and T. This is also illustrated in Fig. 2(b). The maximum dispersion of the curves for the different systems over the whole energy range (even for 0.1 eV) is less than 5%.

The viscosity cross section for both symmetric and asymmetric systems is independent of the reduced mass, and no additional scaling is needed. Thus

$$\sigma_{\mathrm{vi}}^{A+B}(E) = \sigma_{\mathrm{vi}}^{H+H}(E) \tag{41}$$

as illustrated in Fig. 2(c). Again the deviations around H + H curves stay below 5% for energies below 1 eV, becoming negligible at higher energies.

Unlike the $H^+ + H$ case, where $\sigma_{\mathrm{mt,sym}} = 2\sigma_{\mathrm{ct,sym}}$, here we find for the H+H case

$$\sigma_{\mathrm{mt}} \approx 5.2\sigma_{\mathrm{se}}. \tag{42}$$

C. Hydrogen ion-molecule collision systems: $A^+ + BC$

Collisions of hydrogen ions with hydrogen molecules are treated as collisions of distinguishable particles, and thus we do not expect any conceptual difference between the systems, except to account for differences in the reduced masses as well as in the vibrational couplings and energies. Surprisingly, after averaging over the diatomic orientations, the elastic cross sections scale well with the system's reduced mass if only the projectile is varied. For a fixed projectile mass the cross section does not depend significantly on the details of the molecular target, and no scaling is needed, especially if the collision energies are above 0.3 eV. Figure

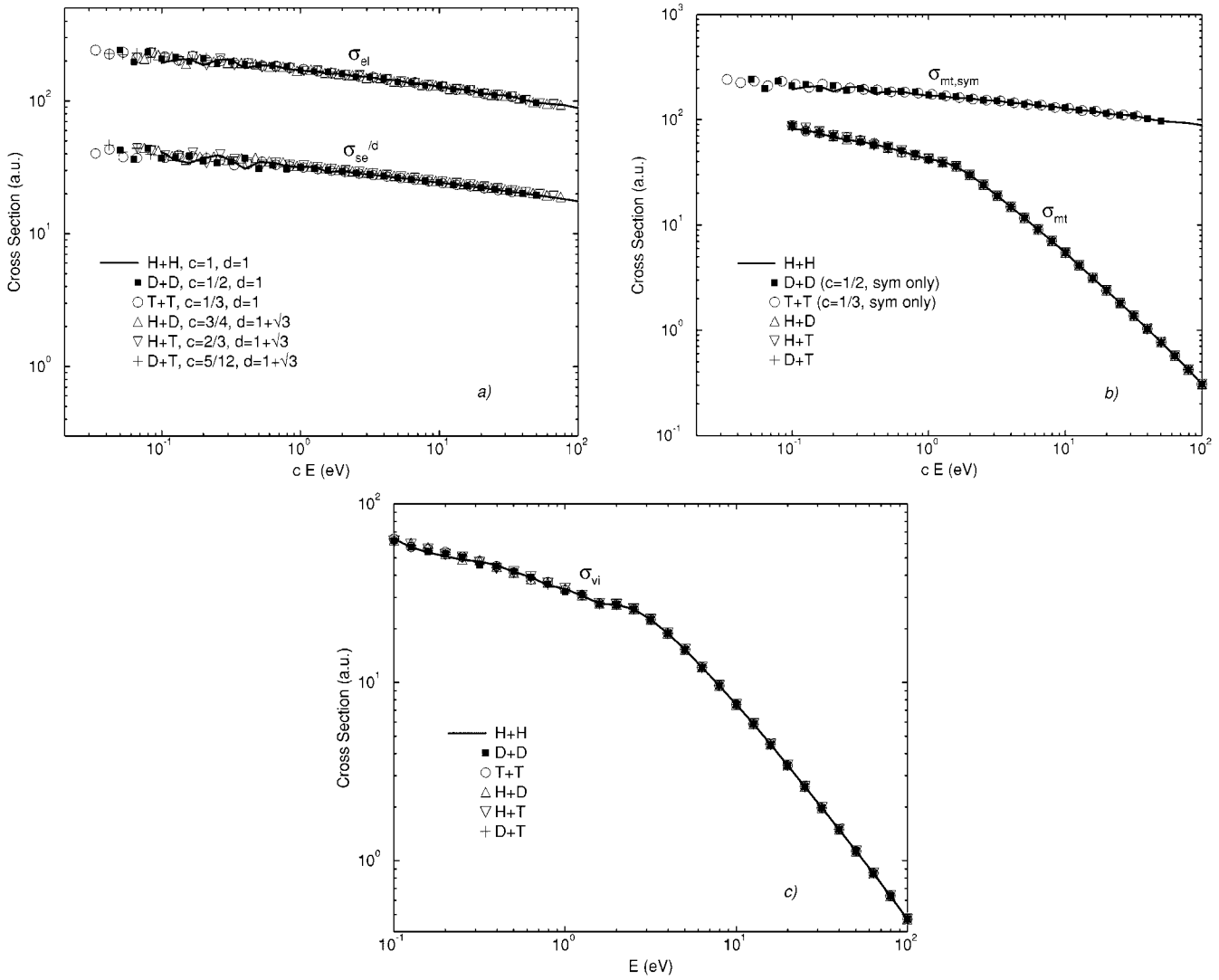

FIG. 2. Scaling of the cross sections for the isotopic variants of hydrogen atom-atom collision systems: (a) elastic (σ_{el}) and spin exchange (σ_{se}); (b) momentum transfer, symmetric ($\sigma_{\mathrm{mt,sym}}$), and asymmetric (σ_{mt}); and (c) viscosity (σ_{vi}). The H+H case is indicated by a solid line.

3(a) illustrates these behaviors, combining various projectiles with all six isotopic combinations of H_2. Thus, for variation of the projectile isotope and for variation of the target isotopomers, respectively, we have

$$\sigma_{\mathrm{el}}^{A^+ + BC}(E) = \sigma_{\mathrm{el}}^{\mathrm{H}^+ + \mathrm{H}_2}\left(\frac{\mu_0}{\mu_{ACD}}E\right), \quad A \neq \mathrm{H},$$
$$\sigma_{\mathrm{el}}^{A^+ + BC}(E) = \sigma_{\mathrm{el}}^{A^+ + \mathrm{H}_2}(E), \tag{43}$$

where μ_0 is the reduced mass of $H^+ + H_2$. The deviations from the $H^+ + H_2$ curve do not exceed 20% over the whole energy range. These drop to less than 5% for energies close to 100 eV, when the collision time becomes short in comparison to the characteristic vibration time of the target.

All the momentum transfer cross sections almost coincide at energies lower than 2 eV [see Fig. 3(b)]. The curves deviate up to a factor of 3 in the range of 10 eV, where the vibrational transitions are most active. This deviation decreases toward higher energies, as with the elastic cross sections, when the momentum transfer cross section becomes very small and population of the vibrational excited states high. The dispersion in that range may also be attributed to possible convergence errors caused by the implemented truncation of the sum over vibrational states, which produces the most pronounced uncertainty for large scattering angles that most affect the momentum transfer cross section. Thus

$$\sigma_{\mathrm{mt}}^{A^+ + BC}(E) = \sigma_{\mathrm{mt}}^{\mathrm{H}^+ + \mathrm{H}_2}(E) \tag{44}$$

for all A, B, and C.

Figure 3(c) shows the viscosity cross sections for all of the isotopic variants. Similar to the momentum transfer case, the curves start to deviate above 2 eV, where the details of vibrational excitations are reflected to the midrange and backward part of the differential cross sections. The deviation decreases toward higher energies. Thus we have

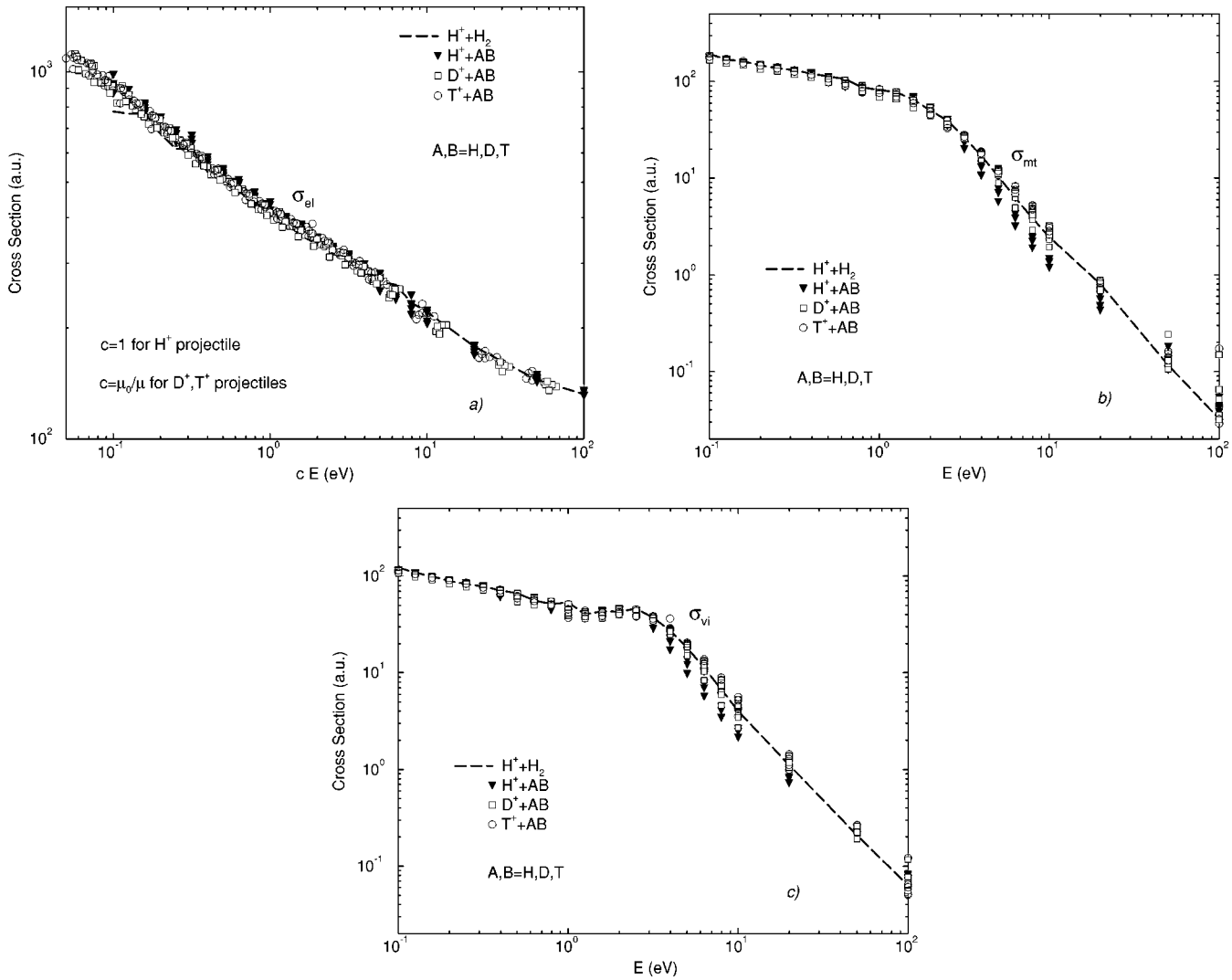

FIG. 3. Scaling of the cross sections for the isotopic variants of hydrogen ion-molecule collision systems: (a) elastic (σ_{el}), (b) momentum transfer (σ_{mt}), and (c) viscosity (σ_{vi}). The $H^+ + H_2$ case is indicated by a dashed line.

$$\sigma_{\mathrm{vi}}^{A^+ + BC}(E) = \sigma_{\mathrm{vi}}^{\mathrm{H}^+ + \mathrm{H}_2}(E) \tag{45}$$

for all A, B, and C.

D. Hydrogen atom-molecule collision systems: $A + BC$

The collisions of neutral atoms with neutral molecules retain the properties similar to cases of ion-molecule systems. Unlike the ion-molecule case, the best scaling is reached for the elastic cross sections if it is performed using the reduced masses for all cases, irrespective of the projectile. This is illustrated in Fig. 4(a). In this case

$$\sigma_{\mathrm{el}}^{A+BC}(E) = \sigma_{\mathrm{el}}^{\mathrm{H}+\mathrm{H}_2}\left(\frac{\mu_0}{\mu_{ABC}}E\right) \tag{46}$$

for all A, B, and C.

The momentum transfer and viscosity cross sections coincide, and no scaling is needed, as shown in Figs. 4(b) and 4(c). Thus

$$\sigma_{\mathrm{mt}}^{A+BC}(E) = \sigma_{\mathrm{mt}}^{\mathrm{H}+\mathrm{H}_2}(E), \quad \sigma_{\mathrm{vi}}^{A+BC}(E) = \sigma_{\mathrm{vi}}^{\mathrm{H}+\mathrm{H}_2}(E). \tag{47}$$

We note that the dispersion of the results is smaller than in the ion-molecule case, and does not exceed 30% in the vibrationally active region of collision energies (except at 100 eV) for both momentum transfer and viscosity cross sections. For the elastic cross section, the deviations are quantitatively similar to the ion-molecule cases.

E. Comparisons among various systems

Figure 5(a) shows a comparison of the elastic cross sections for the four types of systems considered (excluding the isotopic variants of H). The cross sections with correct CDP limits, as defined in the previous sections, are shown. For reference, we also show the QIP cross section ($\sigma_{\mathrm{tot,sym}}$) for $H^+ + H$.

Very surprising is the high level of similarity of H+H and $H + H_2$ cross sections. They stay approximately equal in the whole energy range. Similar also are the cases $H^+ + H$ and $H^+ + H_2$, though to a less extent. The $H^+ + H$ elastic

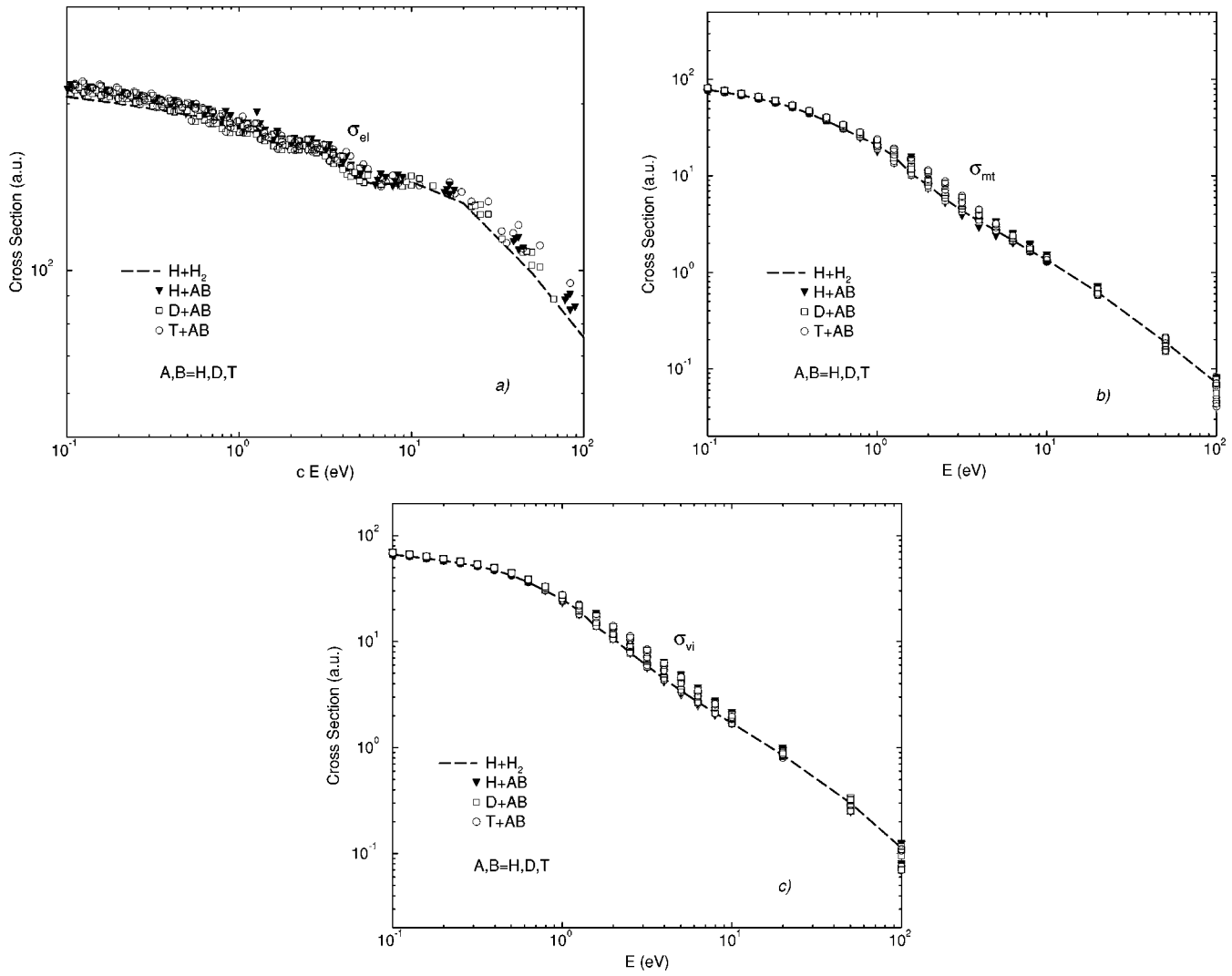

FIG. 4. Scaling of the cross sections for the isotopic variants of hydrogen atom-molecule collision systems: (a) elastic (σ_{el}); (b) momentum transfer (σ_{mt}), and (c) viscosity (σ_{vi}). The $H+H_2$ case is indicated by a dashed line.

cross section is about 2.5 times bigger than that of H + H, for energies of a fraction of eV. With an increase of collision energy, this factor slightly decreases, staying above 2. The QIP cross section for $H^+ + H$ stays more than a factor of 3 bigger than the CDP result for the H+H system. Note that the latter does not contain the recoil scattering contribution. The full QIP elastic cross section for H+H can be simply obtained by multiplication of the elastic cross section by 2.

The comparison of the momentum transfer and viscosity cross sections for the four types of systems is shown in Figs. 5(b) and 5(c). Excluding the cases where QIP is assumed, most of the momentum transfer cross sections for various system types do not deviate from each other by more than a factor of 2. If the QIP momentum transfer cross section for H + H is multiplied by 2 (thus accounting for both direct and recoil channels), this becomes quite close to the QIP momentum transfer cross section for $H^+ + H$.

All CDP viscosity cross sections are very similar for energies lower than 1 eV. At higher energies, when the vibrational excitation channels open, the cases with molecular targets deviate from the ion-atom and atom-atom systems. Finally, at higher energies, close to 100 eV, when the vibrational structure of the molecule plays a lesser role in the collision dynamics, the viscosity cross sections with like projectiles become similar.

IV. CONCLUSIONS

Utilizing comprehensive, very accurate fully quantal calculations of the elastic cross sections for scattering of isotopomers of hydrogen ions, atoms, and molecules over the range of center-of-mass collision energies 0.1–100 eV, we have considered the scaling relations among various groups of collision partners. In addition, we have elucidated consistent definitions of the elastic and common transport related cross sections regarding preservation of the classical distinguishability of particles at high collision energies, while allowing for the quantum indistinguishability of particles, clearing up a number of inconsistent definitions found in the literature.

In particular, we have considered four groups of collision systems: ion-atom, atom-atom, ion-molecule, and atom-molecule. In each group separately we find that, over the whole energy range, the elastic cross sections scale with a simple reduced mass ratio multiplying the CM collision energy, and thus with the square of the CM velocity. The mo-

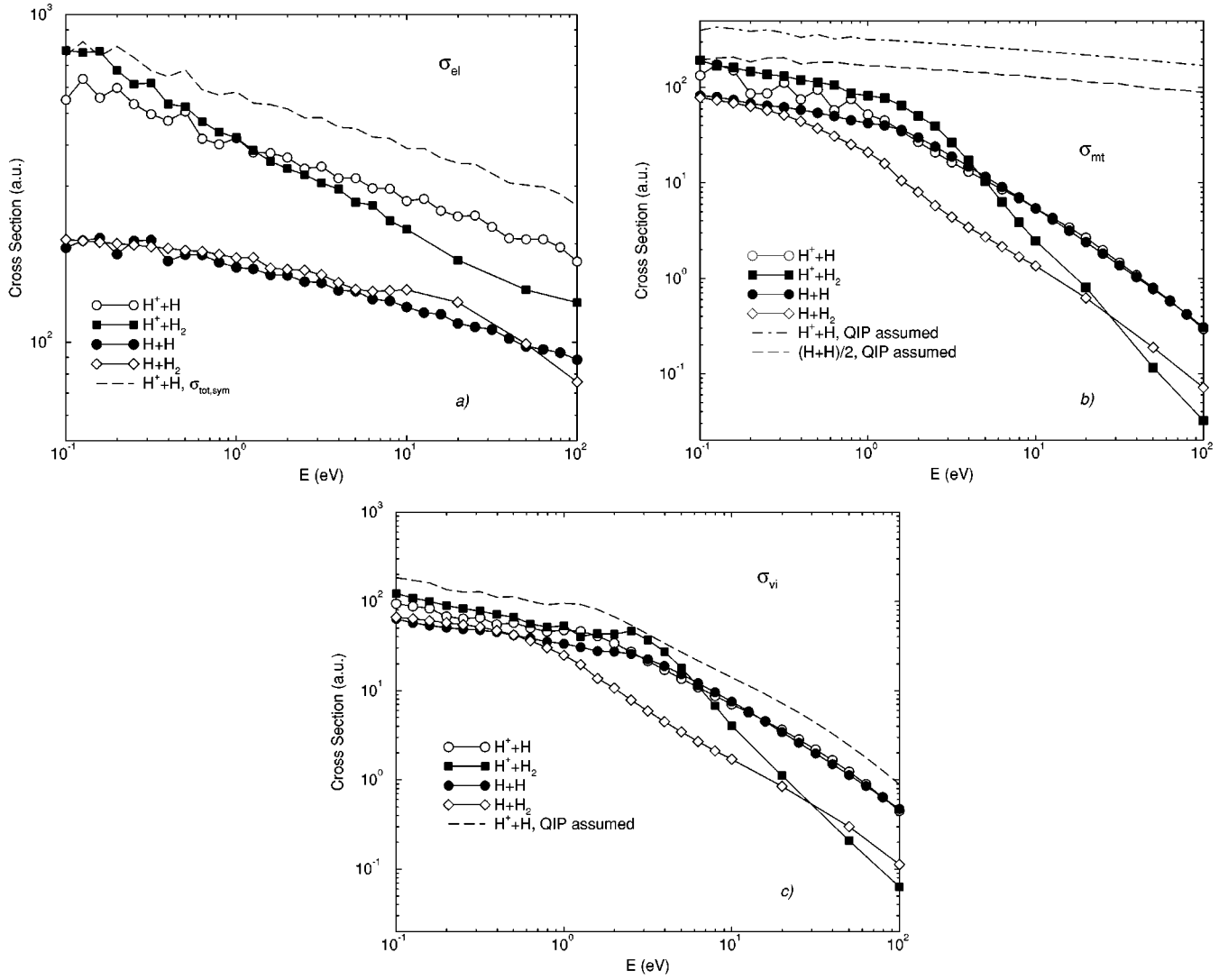

FIG. 5. Comparison of the cross sections for the various classes of collision systems which involve hydrogen ions, atoms, and molecules: (a) elastic (σ_{el}), (b) momentum transfer (σ_{mt}); and (c) viscosity (σ_{vi}).

mentum transfer and viscosity cross sections, on the other hand, are similar within each group, showing independence on both reduced mass and on the vibrational structure (in the case of molecular targets). We also particularly find that the assumption of the classical distinguishability for the isotopically like nuclei in ion-atom and atom-atom cases of hydrogen is an acceptable alternative to the inconsistent definitions of the elastic cross sections for the symmetric and asymmetric systems, in the whole range of energies considered.

ACKNOWLEDGMENTS

This work has been supported by the U.S. Department of Energy, Office of Fusion Energy Sciences, at Oak Ridge National Laboratory, which is managed by the Lockheed Martin Energy Research Corporation under Contract No. DE-AC05-96OR22464. The authors wish to thank Randy Kanzleiter, Daren Stotler, and John Raymond for stimulating comments on the application of elastic scattering data in fusion and astrophysical plasmas.

[1] D. Reiter, P. Bachmann, and A.K. Prinja, Contrib. Plasma Phys. **32**, 261 (1992).
[2] D. Ruzic, Phys. Fluids B **5**, 2140 (1993).
[3] D. Reiter, C. May, D. Coster, and R. Schneider, J. Nucl. Mater. **220-222**, 987 (1995).
[4] D. Ruzic, J. Nucl. Mater. **220-222**, 1091 (1995).
[5] P. Bachmann and D. Reiter, Contrib. Plasma Phys. **35**, 45 (1995).
[6] D.R. Schultz, S.Yu. Ovchinnikov, and S.V. Passovets, in *Atomic and Molecular Processes in Fusion Edge Plasmas*, edited by R.K. Janev (Plenum, New York, 1995), p. 279.
[7] D. Ruzic and D.B. Hayden, Fusion Technol. **31**, 123 (1997); D.B. Hayden and D. Ruzic, *ibid.* **31**, 128 (1997).
[8] R.R. Hodges and E.L. Breig, J. Geophys. Res. **96A**, 7697

(1991).
[9] D.J. Mullan and C.N. Arge, J. Geophys. Res. **101A**, 2535 (1996).
[10] L.L. Williams, D.T. Hall, H.L. Pauls, and G.P. Zank, Ap. J. **476**, 366 (1997).
[11] T.I. Gombosi, K.G. Powell, and D.L. Dezeeuw, J. Geophys. Res. **99A**, 21 525 (1994).
[12] J.M. Laming, J.C. Raymond, B.M. McLaughlin, and W.P. Blair, Ap. J. **472**, 267 (1996).
[13] M.J. Jamieson, A. Dalgarno, and J.N. Yukich, Phys. Rev. A **46**, 6956 (1992).
[14] M.J. Jamieson, A. Dalgarno, B. Zygelman, P.S. Krstić, and D.R. Schultz, Phys. Rev. A (to be published).
[15] B.H. Bransden and M.R.C. McDowell, *Charge Exchange and the Theory of Ion-Atom Collisions* (Clarendon Press, Oxford, 1992).
[16] M.R.C. McDowell and J.P. Coleman, *Introduction to the Theory of Ion-Atom Collisions* (North-Holland, London, 1970).
[17] L.D. Landau and E.M. Lifshitz, *Quantum Mechanics — Non-relativistic Theory* (Pergamon Press, New York, 1965).
[18] J.O. Hirschfelder, C.F. Curtiss, and B.B. Bird, *Molecular Theory of Gases and Liquids* (John Wiley & Sons, New York, 1964).
[19] A.C. Allison and F.J. Smith, At. Data **3**, 317 (1971).
[20] F. Masnou-Seeuvs and A. Salin, J. Phys. B **2**, 1274 (1969).
[21] G. Hunter and M. Kuriyan, At. Data Nucl. Data Tables **25**, 287 (1980).
[22] A. Dalgarno, Proc. R. Soc. London, Ser. A **262**, 132 (1961).
[23] P.S. Krstić and D.R. Schultz, A. Plasma-Mater. Interact. Data Fusion **8**, 1 (1998).
[24] P.S. Krstić and D.R. Schultz, J. Phys. B **32**, 2415 (1999).
[25] B. Johnson, J. Comput. Phys. **13**, 445 (1973).
[26] E.W. McDaniel, *Collision Phenomena in Ionized Gases* (John Wiley & Sons, New York, 1964); *Atomic Collisions: Heavy Particle Projectiles* (John Wiley & Sons, New York, 1993).
[27] M. Abramowitz and I.S. Stegun, *Handbook of Mathematical Functions* (Dover, New York, 1972).
[28] R.J. Damburg and R. Kh. Propin, J. Phys. B **1**, 681 (1968).
[29] E.A. Solov'ev, Usp. Fiz. Nauk **157**, 437 (1989) [Sov. Phys. Usp. **32**, 228 (1989)].
[30] J.H. Macek and K.A. Jerjian, Phys. Rev. A **33**, 233 (1986).
[31] M.J. Jamieson (private communication).
[32] L. Wolniewicz, J. Chem. Phys. **99**, 1851 (1995), and references therein.
[33] M. Baer and H. Nakamura, J. Chem. Phys. **66**, 1363 (1987).
[34] M. Baer, G. Niedner, and J.P. Toennies, J. Chem. Phys. **88**, 1461 (1988); M. Baer, Adv. Chem. Phys. **82**, 401 (1992).
[35] M. Baer, G. Niedner-Schatteburg, and J.P. Toennies, J. Chem. Phys. **91**, 4169 (1989).
[36] M.W. Schmidt, K.K. Baldridge, J.A. Boatz, S.T. Elbert, M.S. Gordon, J.H. Jensen, S. Koseki, N. Matsunaga, K.A. Nguyen, S.J. Su, T.L. Windus, M. Dupuis, and J.A. Montgomery, J. Comput. Chem. **14**, 1347 (1993).
[37] A.I. Boothroyd, W.J. Keogh, P.G. Martin, and M.R. Peterson, J. Chem. Phys. **95**, 4343 (1991).
[38] C.F. Giese and W.R. Gentry, Phys. Rev. A **10**, 2156 (1974).
[39] R. Schinke and P. McGuire, Chem. Phys. **31**, 391 (1978).
[40] R. Schinke, M. Dupuis, and A. Lester, J. Chem. Phys. **72**, 3909 (1980).
[41] G. Neidner, N. Noll, and J.P. Toennies, J. Chem. Phys. **87**, 2685 (1987).
[42] URL: www-cfadc.phy.ornl.gov